Electronic Supplementary Information （ESI）

Stable Terbium Metal-organic Framework with Turn-on and Blue-shift Fluorescence Sensing for Acidic Amino Acids (L-aspartate, L-glutamine) and Cation (Al^{3+}, Ga^{3+})

Tai-Lin Ren, Xiao-Nuan Zhang, Jun-Jie Hu, He-Rui Wen*, Sui-Jun Liu, Yan Peng

School of Chemistry and Chemical Engineering, Jiangxi Provincial Key Laboratory of Functional Molecular Materials Chemistry, Jiangxi University of Science and Technology, Ganzhou 341000, Jiangxi Province, P.R. China.

E-mail: wenherui63@163.com; sjliu@jxust.edu.cn

General Procedures, Materials and Instruments

Materials and Instruments: H_4ADIP, $Tb(NO_3)_3 \cdot 6H_2O$, Formic acid and DMF were used as purchased without further purificaton. Infrared spectra were recorded using an ALPHA (Bruker) spectrophotometer with KBr pellets in the region 4000-400 cm^{-1}. The powder X-ray diffraction (PXRD) spectra were recorded using a Rigaku D/Max-2500 diffractometer with a Cu-target tube. Simulation of the PXRD spectra were carried out by the single-crystal data and diffraction-crystal module of the Mercury (Hg) program was available free of charge via the Internet at *http://www.iucr.org*. Thermogravimetric analysis (TGA) was carried out using a NETZSCH STA2500 (TG/DTA) at a heating rate of 10 °C·min^{-1} under nitrogen atmosphere.

PXRD and IR: The PXRD diffraction peaks of Tb-MOF were consistent with the simulated peaks, which proved the complexe is isostructural and in pure phase (Supporting Information Figure S3a). The IR spectras of MOFs Tb-MOF was showed in Supporting Information Figure S1. The infrared spectra measured at room temperature exhibit a broad absorption band with minimum at 3431 cm^{-1} may be attributed to ν(OH). The positions of the carboxylate bands are in usual region, 1659 cm^{-1} for antisymmetric vibration($\nu_{as}(COO^-)$), 1271 and 1099 cm^{-1} for the symmetric vibrations($\nu_s(COO^-)$). The presence of $(CH_3)_2NH_2^+$ in the channels can be seen from characteristic absorption bands of 2924 cm^{-1} and 2852 cm^{-1}, which correspond to antisymmetric and symmetric aliphatic stretching vibrations of methyl groups.

TGA: The TGA was performed from 25 to 1000 °C under N_2 flow to explore the thermal stability of Tb-MOF. The TG analysis (Supporting Information Figure S3b) indicated that weight loss of 4.7% of MOF Tb-MOF with the temperature ranging from 25 °C to 120 °C, and the reason may be the removal of incomplete drying in the air and lattice water molecules. Weight loss of 14.5% between 120 and 350 °C is probably removed DMF and HCOOH. The decompositions of the framework of complexes began around at 350 °C, indicating the relatively good thermal stability.

Table S1. Selected bond lengths (Å) and angles (deg) for Tb-MOF.

Tb1—O1	2.441(4)	Tb1—O5^{i}	2.291(5)
Tb1—O2	2.311(5)	Tb1—O6^{ii}	2.476(6)
Tb1—O8	2.427(6)	Tb1—O10^{ii}	2.371(6)
Tb1—O9	2.379(7)	Tb1—O12	2.473(6)
O1—Tb1—O6^{ii}	158.09(14)	O8—Tb1—O1	105.3(3)
O1—Tb1—O12	80.62(18)	O8—Tb1—O6^{ii}	77.9(2)
O12—Tb1—O6^{ii}	116.5(2)	O8—Tb1—O12	53.0(2)
O2—Tb1—O1	86.03(19)	O9—Tb1—O1	80.3(2)
O2—Tb1—O8	144.8(2)	O9—Tb1—O8	75.4(3)
O2—Tb1—O9	73.9(3)	O9—Tb1—O6^{ii}	79.6(2)
O2—Tb1—O6^{ii}	80.0(2)	O9—Tb1—O12	116.6(3)
O2—Tb1—O10^{ii}	103.3(2)	O5^{i}—Tb1—O1	76.7(2)
O2—Tb1—O12	161.03(19)	O5^{i}—Tb1—O2	83.0(2)
O5^{i}—Tb1—O6^{ii}	117.8(2)	O5^{i}—Tb1—O8	131.8(2)
O5^{i}—Tb1—O10^{ii}	74.0(2)	O5^{i}—Tb1—O9	148.3(3)
O5^{i}—Tb1—O12	80.9(2)	O10^{ii}—Tb1—O1	147.75(16)
O10^{ii}—Tb1—O6^{ii}	53.23(18)	O10^{ii}—Tb1—O8	84.9(3)

Symmetry codes: (i) -x+1, y, -z+3/2; (ii) x-1/2, -y+1/2, z-1/2; (iii) -x, -y+1, -z+1; (iv) -x+3/2, -y+1/2, -z+1; (v) x+1/2, -y+1/2, z+1/2.

Table S2. Sensing Performance Comparison of Reported Fluorescent MOF Sensors for L-Asp or L-Glu.

Analytes	MOFs	detection process	detection limits (μM)	Ref.
L-Asp	**{[Tb_2(ADIP)(H_2ADIP)(HCOOH)(H_2O)$_2$]·2DMF·2H_2O}$_n$**	**turn-on**	**0.25**	**this work**
	Cu/Tb@Zn-MOF	turn-on	4.05	1
	Ag^+@Eu-complex	turn-on	0.46	2
	1@SA	turn-on	80	3
	Cd_2(idc)(dht)(H_2O)$_4$	turn-on	9.35	4
	[$Cd_{1.5}$(NTB)(bipy)$_{0.5}$]$_n$	turn-off	2.68	5
L-Glu	**{[Tb_2(ADIP)(H_2ADIP)(HCOOH)(H_2O)$_2$]·2DMF·2H_2O}$_n$**	**turn-on**	**0.23**	**this work**
	[$(CH_3)_2NH_2$]$_2$[Tb_6(μ_3-OH)$_8$(BDC-OH)$_6$(H_2O)$_6$] (solv)$_x$	turn-on	3.6	6
	Cd_2(idc)(dht)(H_2O)$_4$	turn-on	11.34	4
	[$Cd_{1.5}$(NTB)(bipy)$_{0.5}$]$_n$	turn-off	130	5
	[Cd(L)(bbibp)]$_n$	turn-off	1.03	7
	[Cd(L)(bbibp)$_{0.5}$]$_n$	turn-off	2.42	7
	{[Cd_2(PPTA)(DMF)$_2$(H_2O)]·2DMF·4H_2O}$_n$	turn-off	0.115	8

Table S3. Sensing Performance Comparison of Reported Fluorescent MOF Sensors for L-Asp or L-Glu.

Analytes	MOFs	detection process	detection limits (μM)	Ref.
Al^{3+}	**$\{[Tb_2(ADIP)(H_2ADIP)(HCOOH)(H_2O)_2]\cdot 2DMF\cdot 2H_2O\}_n$**	**turn-on**	**0.069**	**this work**
	$[Co_2(dmimpym)(nda)_2]_n$	turn-on	0.70	9
	$[Cd(PAM)(4\text{-}bpdb)_{1.5}]\cdot DMF$ (Cd-MOF)	turn-on	0.56	10
	$\{Cd_2(syn\text{-}dftpmcp)(1,3\text{-}BDC)_2\}_{0.5}DMF\cdot H_2O]_n$	turn-off	0.72	11
	$\{[Eu(BTB)(phen)]_{4.5}DMF\cdot 2H_2O\}_n$	turn-off	0.05	12
	$\{[(CH_3)_2NH_2][Eu(BTDB)_2]\cdot 2H_2O\}_n$	turn-on	0.11	13
	$\{[Co_3(BIBT)_3(BTC)_2(H_2O)_2]\cdot solvents\}_n$	turn-on	0.10	14
Ga^{3+}	**$\{[Tb_2(ADIP)(H_2ADIP)(HCOOH)(H_2O)_2]\cdot 2DMF\cdot 2H_2O\}_n$**	**turn-on**	**0.079**	**this work**
	$\{[(CH_3)_2NH_2][Eu(BTDB)_2]\cdot 2H_2O\}_n$	turn-on	0.14	13
	$\{[Zn_2(BBIP)_2(NDC)_2]\cdot H_2O\}$ n	turn-on	9.93	15
	IRMOF-3	turn-on	8.54	16

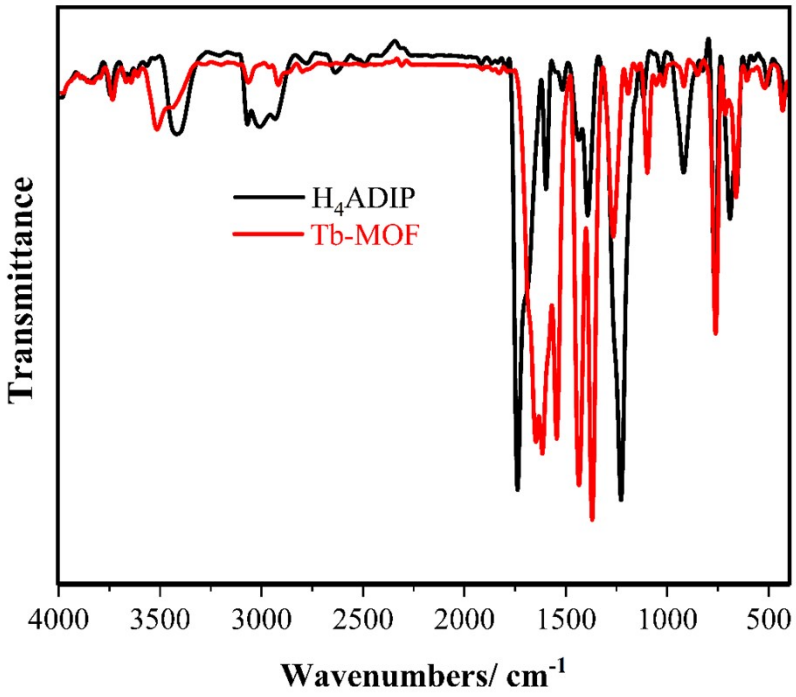

Fig. S1. Infrared spectra of Tb-MOF and H_4ADIP ligand.

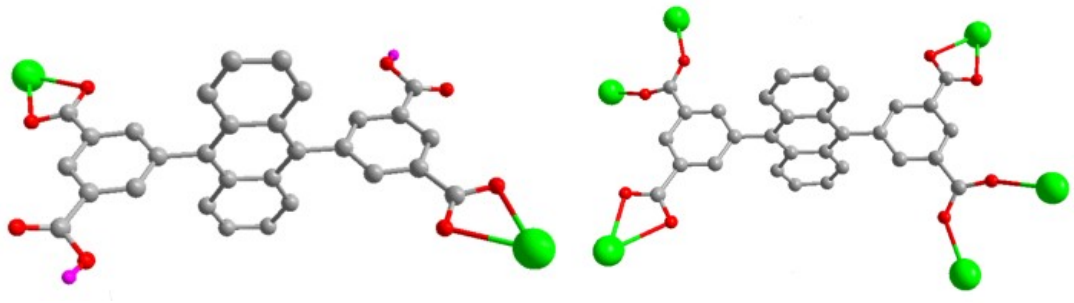

(a) (b)

Fig. S2. (a) H_2ADIP^{2-} coordination mode with Tb^{III} and (b) $ADIP^{4-}$ coordination mode with Tb^{III} ion.

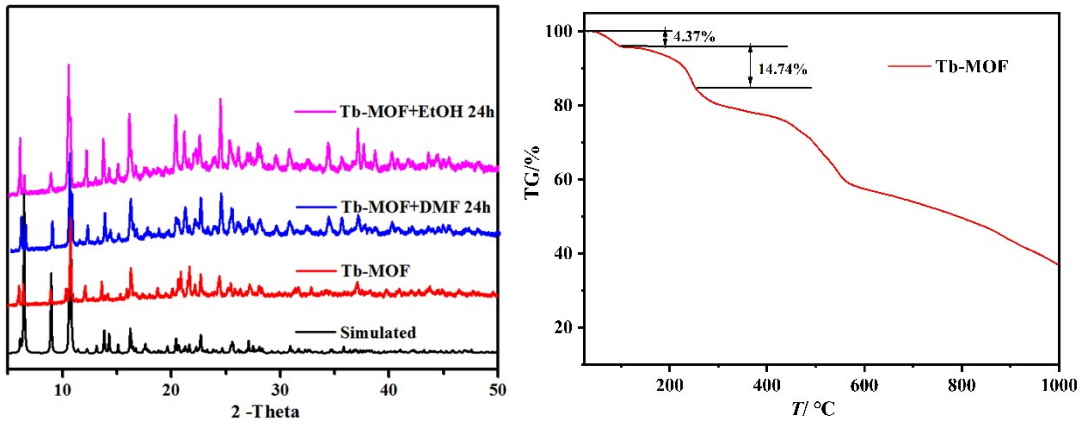

(a) (b)

Fig. S3. (a) The PXRD patterns of Tb-MOF. (b) TG testing of Tb-MOF.

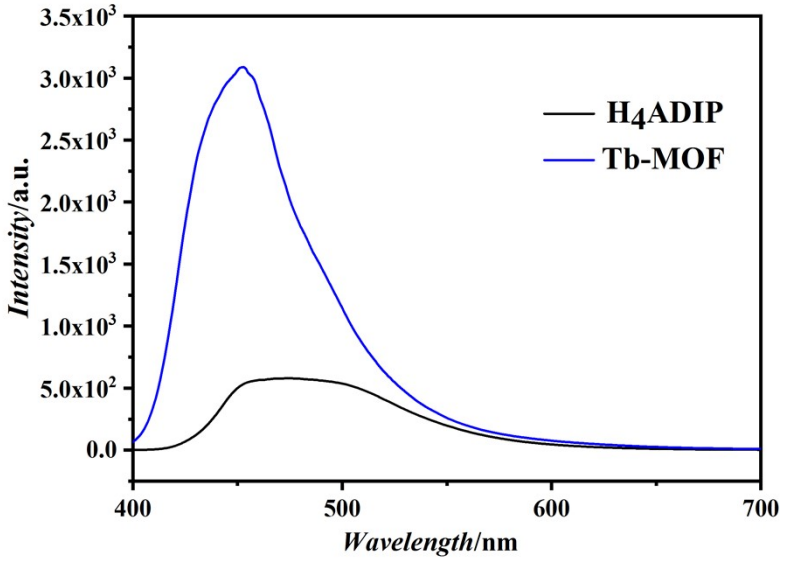

(a)

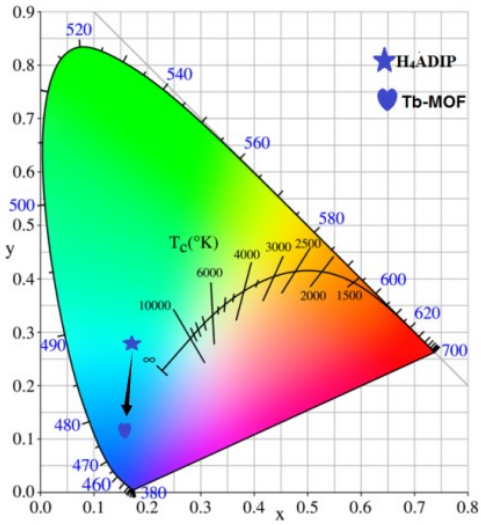

(b)

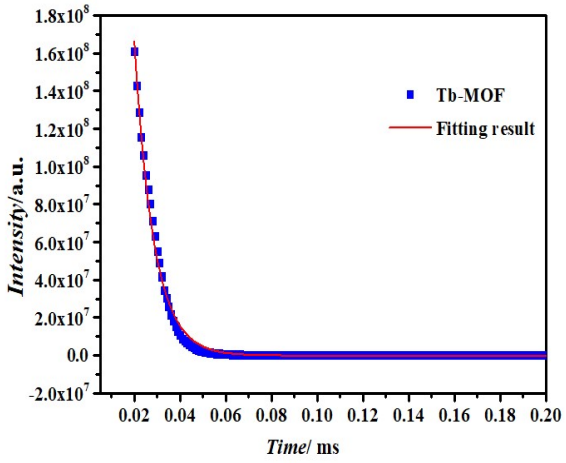

(c)

Fig. S4. (a)The fluorescence emission peaks of H_4ADIP ligand and Tb-MOF. (b) CIE of Tb-MOF. (c) Fluorescence lifetimes of Tb-MOF.

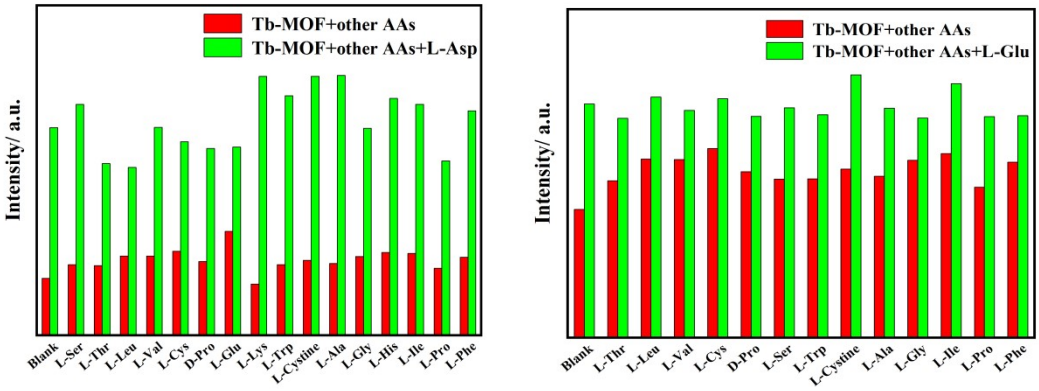

(a) (b)

Fig. S5. Anti-interference properties of Tb-MOF (a) for L-Asp and (b) for L-Glu.

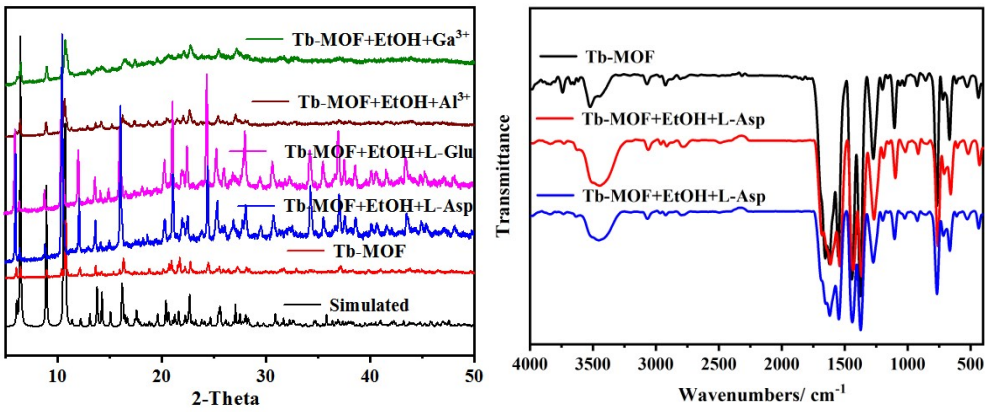

(a) (b)

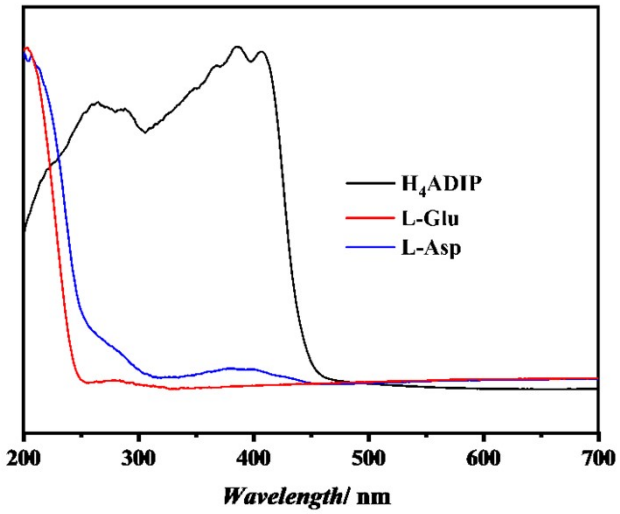

(c)

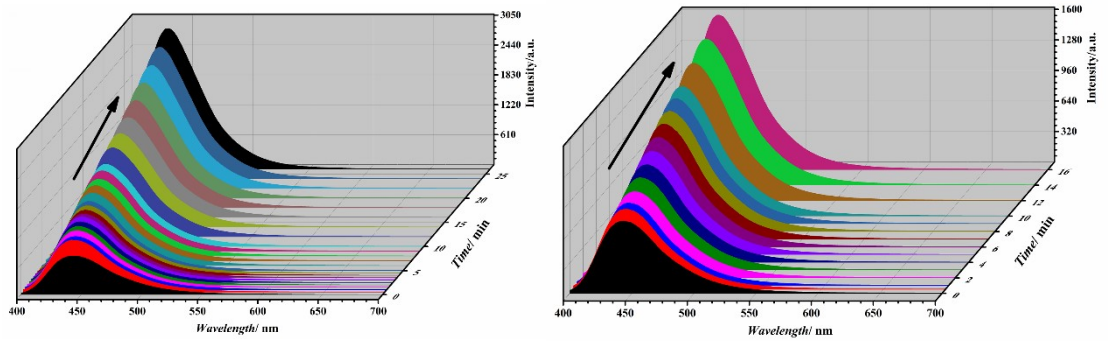

(d) (e)

Fig. S6. (a) The PXRD spectra of Tb-MOF immersed in ethanol solution of Al^{3+} ion, Ga^{3+} ion, L-Asp or L-Glu for 24 h. (b) Infrared spectra of Tb-MOF immersed in ethanol solution of L-Asp or L-Glu for 24 h. (c) Solid-state UV absorption spectra of H_4ADIP, L-Asp and L-Glu. Time response diagram (d) for L-Asp and (e) for L-Glu

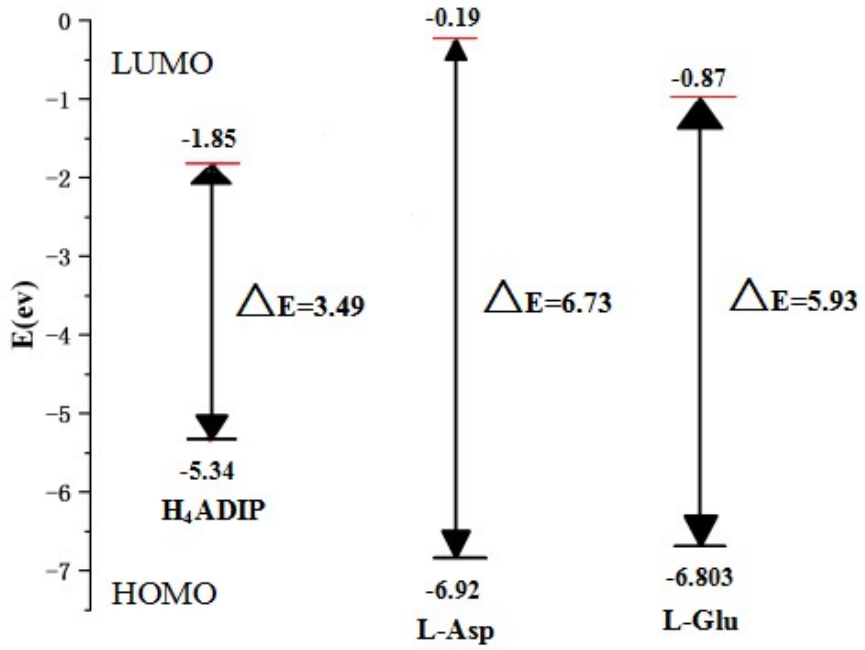

Fig. S7. HOMO−LUMO energy band gaps for H_4ADIP、L-Asp and L-Glu.

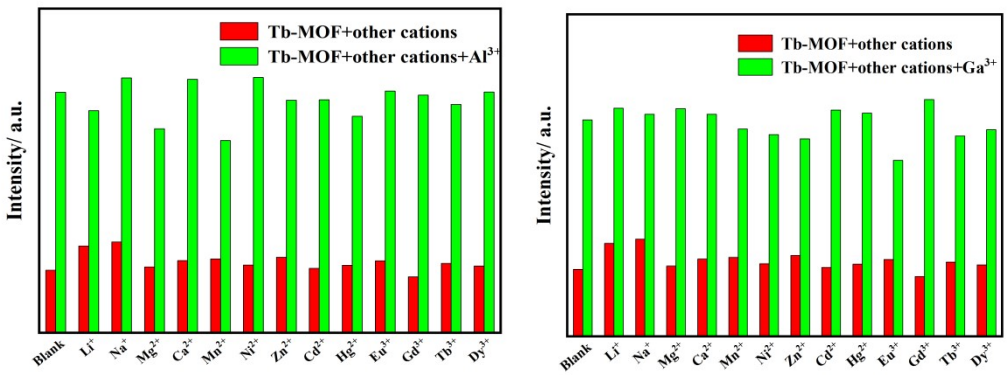

Fig. S8. Anti-interference properties of Tb-MOF (a) for Al^{3+} ion and (b) for Ga^{3+} ion.

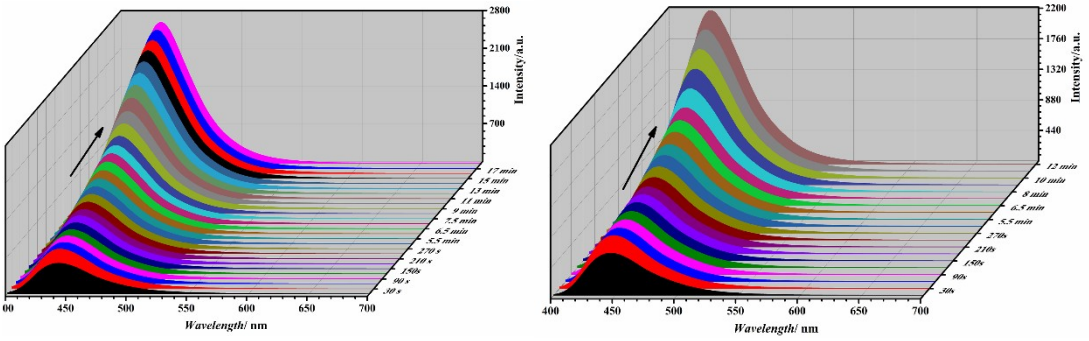

(a) (b)

Fig. S9. Time response diagram (a) for Al^{3+} ion and (b) for Ga^{3+} ion.

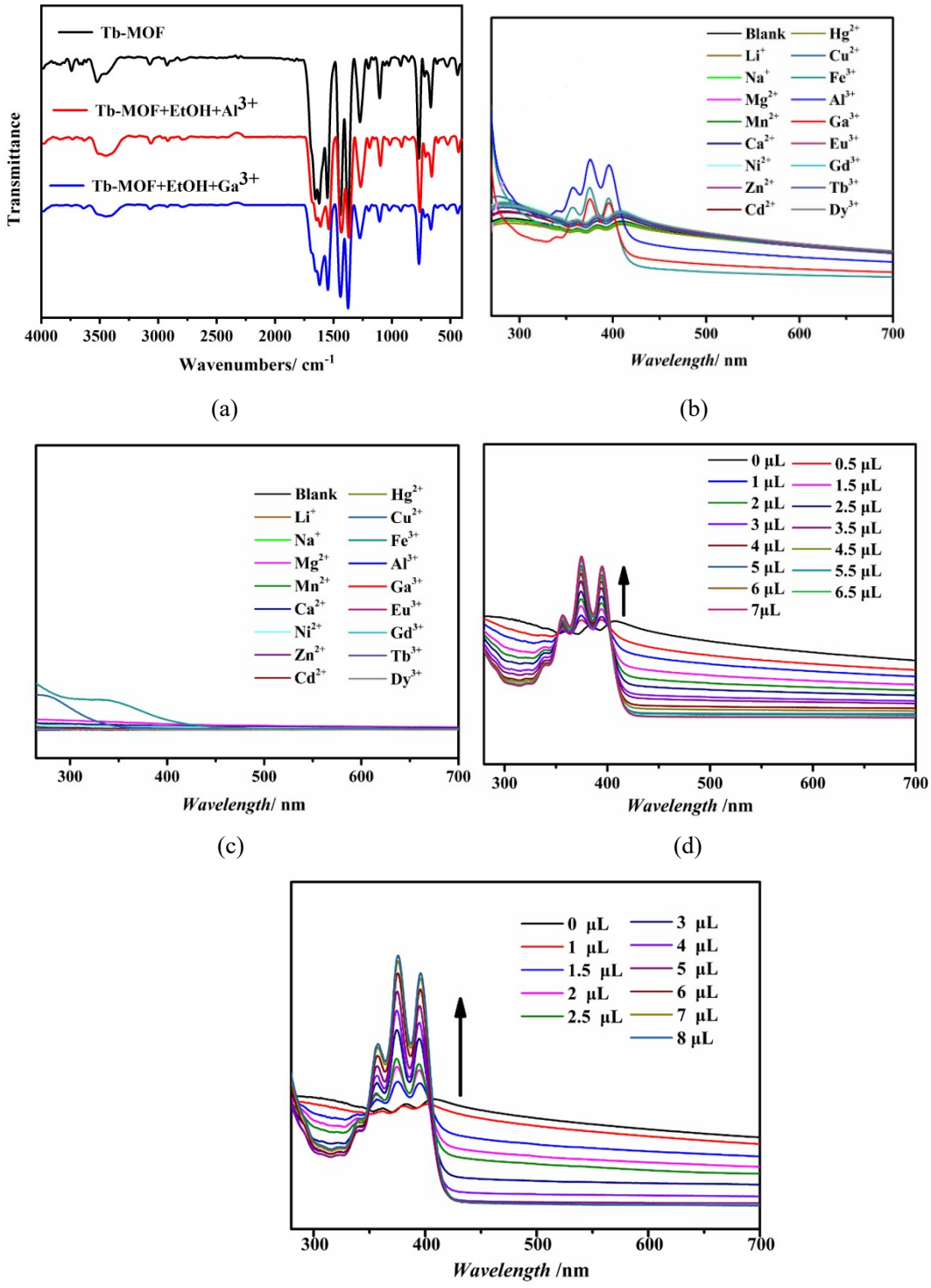

Fig. S10. (a) Infrared spectra of Tb-MOF immersed in ethanol solution of Al^{3+} ion or Ga^{3+} ion for 24 h. (b) Excitation spectra of Tb-MOF and UV absorption spectra of cations solution. (c) UV absorption spectra of cations in EtOH solution. UV absorption spectra of (d) Al^{3+} ion and (e) Ga^{3+} ion added dropwise to Tb-MOF suspension with different concentrations.

References

1 G. Ji, T. Zheng, X. Gao and Z. Liu, *Sens Actuators B Chem.*, 2019, **284**, 91–95.

2 H. Weng and B. Yan, *Sens Actuators B Chem.*, 2017, **253**, 1006–1011.
3 H. Sha and B. Yan, *J Mater Chem C*., 2022, **10**, 7633-7640.
4 J. Othong, J. Boonmak, A. Cheansirisomboon, T. Puangmali, W. Phanchai and S. Youngme, *Anal Chim Acta*., 2021, **1187**, 339157.
5 H. Yang, D. Qi, X. Si, Z. Yan, L. Guo, C. Shao, W. Zhang and L. Yang, *J Solid State Chem*., 2022, **310**, 123008.
6 T. Xia, Y. Wan, Y. Li and J. Zhang, *Inorg Chem.*, 2020, **59**, 8809–8817.
7 C. Fan, B. Zhu, X. Zhang, C. Bi, D. Zhang, Z. Zong and Y. Fan, *Inorg Chem.*, 2021, **60**, 6339–6348.
8 Z. H. Jiao, X. L. Jiang, S. L. Hou, M. H. Tang and B. Zhao, *Inorg Chem.*, 2020, **59**, 2171–2177.
9 W. M. Chen, X. L. Meng, G. L. Zhuang, Z. Wang, M. Kurmoo, Q. Q. Zhao, X. P. Wang, B. Shan, C. H. Tung and D. Sun, *J Mater Chem A.*, 2017, **5**, 13079–13085.
10 R. Lv, Z. Chen, X. Fu, B. Yang, H. Li, J. Su, W. Gu and X. Liu, *J. Solid State Chem*., 2018, **259,** 67–72.
11 W. X. Li, J. H. Gu, H. X. Li, M. Dai, D. J. Young, H. Y. Li and J. P. Lang, *Inorg. Chem*., 2018, **57**, 13453–13460.
12 H. Xu, B. Zhai, C. S. Cao and B. Zhao, *Inorg. Chem.*, 2016, **55**, 9671–9676.
13 J. Li, Y. Zhu, H. Xu, T. F. Zheng, S. J. Liu, Y. Wu, J. L. Chen, Y. Q. Chen and H. R. Wen, *Inorg. Chem.*, 2022, **61**, 3607–3615.
14 X. M. Tian, S. L. Yao, C. Q. Qiu, T. F. Zheng, Y. Q. Chen, H. Huang, J. L. Chen, S. J. Liu and H. R. Wen, *Inorg. Chem.*, 2020, **59**, 2803–2810.
15 L. Wu, S. Yao, H. Xu, T. Zheng, S. Liu, J. Chen, N. Li and H. Wen, *Chinese Chemical Letters.*, 2022, **33**, 541–546.
16 M. Wang, L. Guo and D. Cao, *Sens Actuators B Chem.*, 2018, **256**, 839–845.